ACS OMEGA

http://pubs.acs.org/journal/acsodf

Article

# Effects of Different End Functional Groups Hyperbranched Polymers-Modified Carbon Nanotubes on the Crystallization and Mechanical Properties of Poly(L-lactic acid) (PLLA)

Bofan Shen, Yuxin Xu, Yue Zhang, Zhihui Xie,* Fuyi Zhang, Jian Kang,* Ya Cao, and Ming Xiang

Cite This: *ACS Omega* 2022, 7, 42939−42948

Read Online

ACCESS | Metrics & More | Article Recommendations

**ABSTRACT:** Poly-L-lactic acid (PLLA) is a biodegradable polymer with great mechanical properties and good transparency, but its low crystallization rate greatly limits its application. Hyperbranched polyesters (HBPs) modified carbon nanotubes (CNTs) are an ideal nucleating agent to prove the crystallization of PLLA. To compare different terminal group HBPs' effect on the modification of CNTs and the crystallization of PLLA, through the condensation reaction and amidation reaction, CNTs-H202 and CNTs-N102 were prepared, respectively. The modification was confirmed by Fourier-transform infrared (FTIR) spectroscopy, X-ray electron spectroscopy (XPS), and thermogravimetric analysis (TGA). Using transmission electron microscopy (TEM), we observed the changes on the surface of modified CNTs. PLLA/CNT composites were prepared, and differential scanning calorimetry (DSC) was used to investigate the crystallization behavior of the composites. The mechanical properties of PLLA/CNT composites were investigated as well. The results showed that the modified CNTs had a better promotion on PLLA crystallization and mechanical properties than the unmodified CNTs. CNTs-N102 had a slight advantage on the promotion on PLLA crystallization, which was caused by the lower grafting rate of HBP N102, and CNTs-H202 had a better promotion on the mechanical properties of PLLA, which was caused by the better compatibility with PLLA. In conclusion, hydroxy-terminated HBP is a better CNT modified material than amino-terminated HBP.

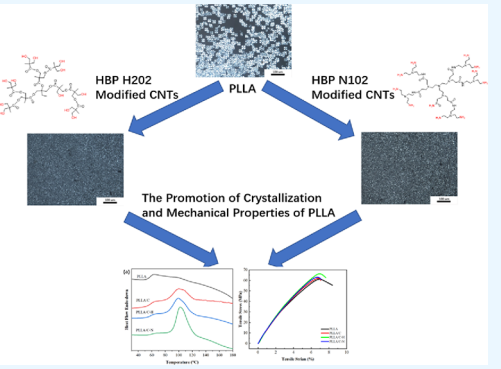


## 1. INTRODUCTION

Poly-L-lactic acid (PLLA) is a biodegradable polymer[1] and thermoplastic aliphatic polyester with high modulus, high strength, and good transparency.[2] In recent decades, PLLA has rapidly emerged as a potential commercial material. Because of its environmentally friendly characteristics, PLLA has become a potential substitute for petroleum-based commodity packaging materials in the hope of reducing white pollution and achieving sustainable development.[3,4] However, in the process of using PLLA materials, people found that PLLA has a low softening temperature and slow crystallization rate,[5] which cannot meet the needs of commercial use.[5,6] Therefore, the efficient regulation of PLLA's crystallization rate which could improve the mechanical properties of the material has become a research hotspot. Great efforts have been made in this field, and results have revealed that a nucleating agent is an ideal solution to improve production efficiency, refine grain size, and increase mechanical strength.[7] The addition of a nucleating agent can reduce the induction time, increase the primary nucleating sites of crystals to refine the grains, and improve the crystallization rate and crystallinity.[8]

Carbon nanotubes (CNTs) have a number of remarkable properties, such as conductivity, heat conduction, and excellent tensile strength, and have attracted extensive attention in many fields such as nanomaterials, composite materials, and biomedical materials.[9−11] As a new type of high-strength and high-modulus nanofiller, CNTs can not only refine the grain and improve the crystallization rate with a small amount of addition but also benefit the mechanical properties of the polymer.[12,13] Therefore, previous studies have used CNTs to regulate the crystallization of PLLA. Wang et al.[14] used CNTs as nucleating agents of polylactic acid (PLA) to prepare CNT/PLA composites, and the results showed that the spherulite size of PLA was significantly reduced after the addition of CNTs. However, in the actual application process, because of the high surface energy of CNTs, agglomeration occurs in the mixing process, which ultimately plays a limited strengthening role or reduces the original properties of the material.[15] On the

Received: August 9, 2022
Accepted: November 2, 2022
Published: November 16, 2022

Scheme 1. Chemical Structure of HBP H202 (Left) and N102 (Right)

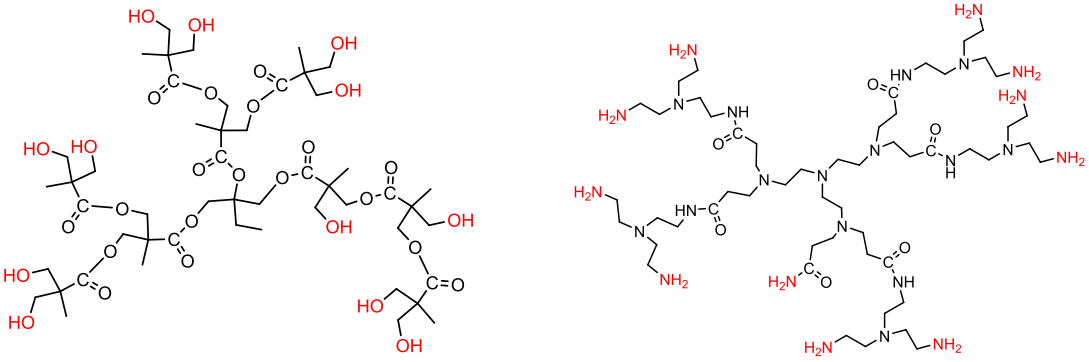

basis of the above issues, the current researchers propose that the surface modification of CNTs could solve this problem.[16]

At present, the modification of CNTs is mainly focused on a small molecule compound and long chain polymer. A small molecule compound usually has few functional groups and limited bonding ability with a polymer matrix. Grafting with a long chain polymer makes the CNTs more compatible with the matrix, but the reaction is often complicated. Whether there are materials that can be simply grafted onto the surface of CNTs with many functional groups, we thought of hyperbranched resins.

Hyperbranched polyesters (HBPs), compared with traditional linear polymers, have the advantages of a low viscosity, high solubility, and a large number of terminal functional groups, and the steric hindrance effect of HBPs might efficiently reduce the agglomeration of CNTs effectively.[17,18] Interestingly, HBPs have been added to PLLA, and the addition of HBPs has been found to efficiently regulate the crystallization of PLLA.[19,20] Therefore, HBPs could be potentially used as ideal modification materials for CNTs. However, HBP can be divided into many types based on different terminal groups. At present, the ability of HBP with different terminal groups to modify CNTs and the effects of modified CNTs on the crystallization and mechanical properties of PLLA have not been studied clearly.[21] Therefore, it is still not clear which terminal group HBP has the best modification effect on CNTs and the regulation of PLLA crystallization. As far as we know, this has not been reported before.

On the basis of these, we selected HBP with a hydroxyl terminal group and HBP with an amino terminal group to modify CNTs, respectively; studied their regulation behavior on PLLA crystallization properties; compared the mechanical properties of different PLLA/CNT composites; and summarized the HBP materials that are more suitable for CNT modification.

## 2. EXPERIMENTAL SECTION

**2.1. Materials and Sample Preparation.** *2.1.1. Materials.* PLLA 4032D was produced by Natureworks Co., Ltd., Minnetonka, MN, USA. The average molecular weight ($M_w$) of PLLA 4032D is $2 \times 10^5$ g/mol, and its melting index is 5.7 g/10 min.[22] The hyperbranched polymers H202 and N102 were purchased from Wuhan Hyperbranched Resin Technology Co., Ltd., China. The molecular weight of the hyperbranched polymers H202 and N102 are 1200 and 1000 g/mol, respectively. The similar molecular weights of different HBPs weaken the influence of grafting rate of modified CNTs, making the experimental results more focused on the influence of HBP with different end groups modified CNTs on the crystallization performance of PLLA. The hydroxyl content of H202 is 10−12 mol/mol, and the amino content of N102 is 7−9 mol/mol. Their chemical structures are illustrated in Scheme 1. The pure carbon nanotubes and carboxylated high-purity multiwalled carbon nanotubes were produced by Beijing Boyu High-Tech New Materials Technology Co., Ltd., Beijing, China. The carboxylated carbon nanotubes were produced by the chemical vapor deposition (CVD) method, which were catalyzed by natural gas and cobalt catalysts and then oxidized by $KMnO_4$ in $H_2SO_4$ solution at a certain temperature. Tetrabutylammonium bromide (TBAB), *N,N′*-dicyclohexyl carbon imide (DCC), and *N,N′*-dimethylformamide (DMF) were purchased from Chengdu Changlian Chemical Reagent Co., Ltd., Chengdu, Sichuan, China, and ethanol was purchased from Chengdu Dingsheng Era Technology Co., Ltd., Chengdu, Sichuan, China. Deionized water was self-made in the laboratory. The phenolic antioxidant Irganox 1010 was produced by BASF China Co., Ltd., Shanghai, China.

*2.1.2. Preparation of Modified CNTs.* HBP H202-modified CNTs were prepared by the following steps: The carboxylated high-purity multiwalled carbon nanotubes and HBP H202 were vacuum dried at 60 °C for 24 h before use. We added 1 g of carboxylated CNTs, 5 g of HBP H202, and 1 g of TBAB into a 500 mL beaker. Then, we stirred and dissolved the mixture by 200 mL of DMF. An ultrasonic dispersing machine was used to ensure that it was mixed evenly. The solution was then poured into a round-bottomed flask and refluxed at 120 °C for 24 h under magnetic agitation. The product was filtered by a PVDF membrane with a pore size of 0.22 $\mu$m and washed with ethanol and deionized water several times to remove the unreacted HBP H1202 and the impurities generated by the reaction. Finally, CNTs modified by HBP H202 were prepared by vacuum drying at 60 °C for 24 h.

The preparation of HBP N102-modified CNTs was similar to the preparation of HBP H202-modified CNTs. The carboxylated CNTs and HBP N102 were vacuum dried at 60 °C for 24 h before use. HBP N102 was added to the molecular sieve to absorb water and small molecular impurities. We added 1 g of DCC and 1 g of carboxylated CNTs into a 250 mL beaker. This was stirred and dissolved in 5 g of HBP N102 in 150 mL of DMF, and then CNTs and DCC were mixed with DMF solution dissolved with HBP N102. An ultrasonic dispersing machine was used to ensure that it was mixed evenly. The solution was then poured into a round-bottomed flask and refluxed at 90 °C for 24 h under magnetic agitation. The product was filtered by a PVDF



https://doi.org/10.1021/acsomega.2c05104
ACS Omega 2022, 7, 42939−42948

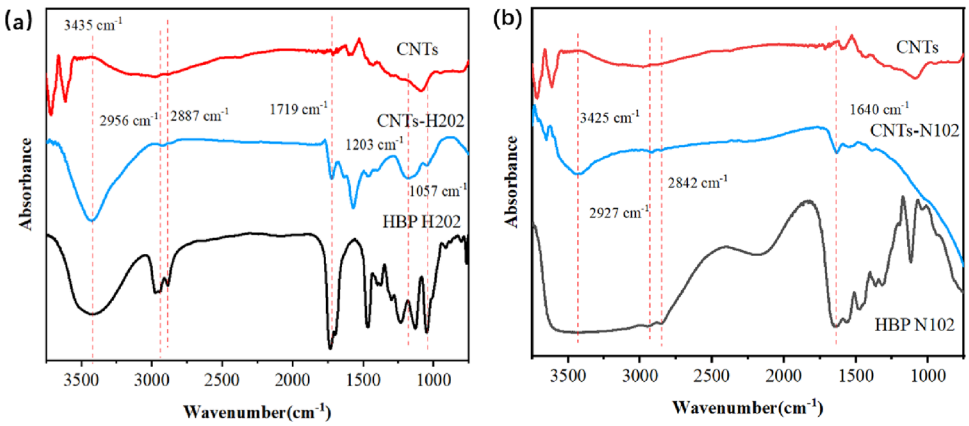


**Figure 1.** (a) FTIR spectra of CNTs, CNTs-H202, and HBP H202. (b) FTIR spectra of CNTs, CNTs-N102, and HBP N102.

membrane with a pore size of 0.22 $\mu$m and washed with ethanol and deionized water several times to remove the unreacted HBP N102 and the impurities generated by the reaction. Finally, CNTs modified by HBP N102 were prepared by vacuum drying at 60 °C for 24 h.

*2.1.3. Preparation of PLLA/CNT Composites.* To explore the influence of modified CNTs on the crystallization properties of PLLA, we prepared pure PLLA and PLLA composites with unmodified CNTs, HBP H202-modified CNTs, and HBP N102-modified CNTs, which were named PLLA, PLLA/C, PLLA/C-H, and PLLA/C-N, respectively. In the composites, according to the previous research, we discussed the effect of the concentration of CNTs on the crystallization of PLLA, and the results showed that the 1 wt % concentration of CNTs has the best regularity on the crystallization of PLLA.[23] Therefore, the concentration of unmodified CNTs, HBP H202-modified CNTs, and HBP N102-modified CNTs is 1 wt %.

Taking sample PLLA/C-H as an example, the pre-vacuum-dried PLLA (40 g) and HBP H202 (0.4 g) were slowly added to the RM-200C torque rheometer with mixing accessories, and they were plasticized for 5 min at 200 °C in the mixing chamber. The compound was then densified at 50 rpm for 10 min in the chamber at 200 °C. To prevent degradation during the dense refining process and reduce the molecular weight, a 1 wt % phenolic antioxidant (Irganox 1010) was added to the dense refining chamber. To facilitate subsequent testing, the samples were made into sheets after refining; the process was carried out as follows: After vacuum drying, the composite was pressed at 200 °C and 10 MPa for 6 min by a hot press, during which three rounds of exhaust operation were required. After pressing the composite into sheets with a thickness of 1 mm, the composite was pressed at room temperature with the same pressure for 4 min to ensure the uniformity of thickness of the composite sheet.

**2.2. Characterization.** *2.2.1. Fourier-Transform Infrared (FTIR) Spectroscopy.* Fourier-transform infrared spectra were recorded on a Nicolet 560 (Nicolet Co., USA) Fourier transform infrared spectrometer at wavelengths ranging from 400 to 4000 $cm^{-1}$ and a resolution of 4 $cm^{-1}$.

*2.2.2. X-ray Photoelectron Spectroscopy (XPS).* An Axis Ultra DLD X Photoelectron spectrometer (Kratos, U.K.) was used to characterize the C, N, and O content of the sample. The X-ray source uses a single Al K$\alpha$ ray with an energy of 1486.6 eV and a voltage of 15 kV. The XPS sensitivity factor quantitative method was used to analyze the content of carbon and oxygen atoms in the samples calculated by the following formula:

$$C_x = \frac{A_x/S_x}{\sum A_i/S_i}$$

where $C_x$ is the concentration of the element on the surface, $A_x$ is the proportion of the element peak, $S_x$ is the sensitivity factor of the element peak, and $\sum A_i/S_i$ is the sum of the ratio of the peak proportion of all elements to the corresponding sensitivity factor. The sensitivity factor of $C_{1s}$ is 0.278, that of $O_{1s}$ is 0.780, and that of $N_{1s}$ is 0.477.[24]

*2.2.3. Thermogravimetric Analysis (TGA).* The HBP H202 and HBP N102 content grafted onto the surface of CNTs was measured using a TG209F1 thermogravimetric analyzer (Netzsch Co., Germany) at a rate of 10 °C/min in a nitrogen atmosphere ranging from 25 to 800 ° C.

*2.2.4. Transmission Electron Microscopy (TEM).* A Tecnai G2 F20 transmission electron microscope (FEI, USA)was used to describe the morphology characterization of CNTs, CNTs-H202, and CNTs-N102 with an acceleration voltage of 200 kV and a two-point resolution of 0.24 nm.

*2.2.5. Wide-Angle X-ray Diffraction (WAXD).* An Ultima IV X-ray diffractometer (Rigaku Co., Japan) was used to detect the samples. Cu K$\alpha$ rays were used as the light source, with wavelength $\lambda$ = 1.54 A, emission voltage 40 kV, current 100 mA, and scanning range $2\theta$ = 5−50°.

*2.2.6. Differential Scanning Calorimetry (DSC).* DSC 3+ (Mettler Toledo Co., Swiss) was used to conduct differential thermal analysis on the composite materials. The samples of the predried composite materials were chopped up and placed in an aluminum crucible with about 4 mg. The samples were heated to 200 °C in a nitrogen atmosphere, kept for 8 min to eliminate the thermal history, and then cooled to 25 °C at rate of 4 °C/min. The calorimetric curve was the crystallization curve, and then the temperature was raised at rate of 10 °C/min, and the calorimetric curve was the melting curve. The crystallinity $X$ of PLLA and its composites was calculated according to the following equation,[25]

$$X = (\Delta H_m - \Delta H_{cc})/\Delta H_f^0$$

where $\Delta H_{cc}$ is the enthalpy of crystallization during PLLA cooling, $\Delta H_m$ is the enthalpy of fusion, and $\Delta H_f^0$ is the melting enthalpy of PLLA with infinite crystal thickness.[26]

The isothermal crystallization process sample preparation was the same as cooling crystallization, but the DSC program



https://doi.org/10.1021/acsomega.2c05104
ACS Omega 2022, 7, 42939−42948

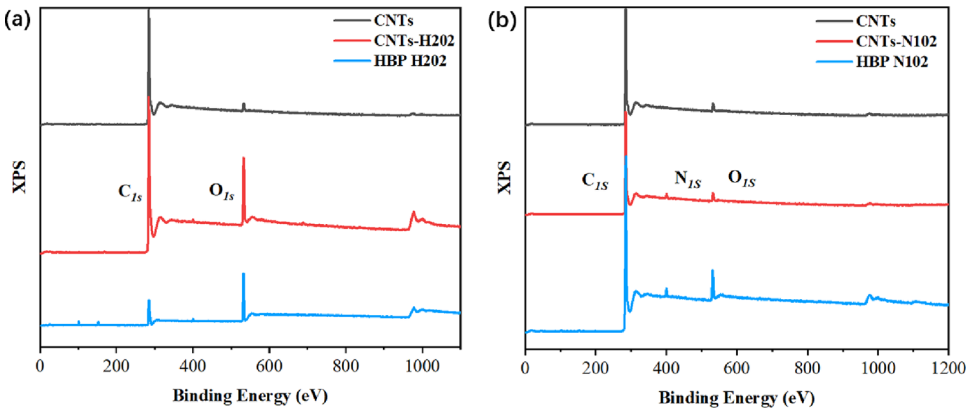


**Figure 2.** (a) XPS survey spectra of CNTs, CNTs-H202, and HBP H202. (b) XPS survey spectra of CNTs, CNTs-N102, and HBP N102.

setting was different. The sample of about 4 mg was heated to 200 °C and kept at 200 °C for 8 min. The purpose was to eliminate the crystal structure in the sample and create the same thermal history for the composite material. Then, it was cooled to 120 °C at a cooling rate of 50 °C/min and kept for 40 min to record the calorimetric curve.

*2.2.7. Polarized Optical Microscopy (PLOM).* The isothermal crystallization process of PLLA and its composites was observed using a Nikon Eclipse LV100N polarizing microscope (Nikon Co., Japan).

*2.2.8. Tensile Property Analysis.* An Instron 5967 universal material testing machine was used for tensile testing. To ensure the uniformity of the tested samples, a MiniJet-Pro (Thermo-Fisher, USA) microinjection molding was used to prepare the samples. The dry sample was placed into the plasticizing chamber of the microinjection molding instrument at 190 °C for 7 min, the mold temperature was set at 80 °C, the injection pressure was 500 bar, the injection time was 10 s, the pressure holding pressure was 300 bar, the time was 10 s, and the dumbbell type stretch spline was prepared with a thickness of about 2 mm and a width of about 4 mm. The tensile process was carried out at room temperature, and the tensile rate was 5 mm/min. The original sample distance was set at 25 mm.

## 3. RESULTS AND DISCUSSIONS

**3.1. Characterization of CNTs.** *3.1.1. FTIR.* The FTIR spectra of pure CNTs, modified CNTs, and HBPs are shown in Figure 1. As shown in Figure 1a, HBP H202 has a broad absorption peak at 3435 $cm^{-1}$, which is the tensile vibration peak of hydroxyl (−OH) in the hyperbranched polyester. The peaks at 2956 and 2887 $cm^{-1}$ represent the antisymmetric and symmetric stretching vibrations of methyl ($-CH_3$) and methylene ($-CH_2-$) groups, respectively. The peak value at 1719 $cm^{-1}$ represents the stretching vibration of the carbonyl group (C═O). Compared with CNTs and CNTs-H202, CNTs-H202 shows a hydroxyl peak at 3435 $cm^{-1}$ and a carbonyl peak at 1719 $cm^{-1}$, indicating that HBP H202 was successfully grafted onto the surface of CNTs. The strong peak values of CNTs-H202 at 2956 and 2887 $cm^{-1}$ also indicate successful surface modification. In addition, the peaks of 1203 and 1057 $cm^{-1}$ are the tensile vibration absorption peaks of C═O and C−O−C, respectively, which are the characteristic absorption peaks of the ester group, indicating the success of esterification reaction.

As shown in Figure 1b, for HBP N102, its N−H wide tensile vibration peak is 3000−3700 $cm^{-1}$, which proves that HBP N102 contains a large amount of $-NH_2$. The two peaks at 2927 and 2842 $cm^{-1}$ are caused by the asymmetric and symmetric vibrations of $-CH_3$ and $-CH_2-$. There is an obvious first-order amide vibration absorption peak at 1640 $cm^{-1}$, and the absorption peak at 3425 $cm^{-1}$ is a second-order amide vibration absorption peak. In conclusion, HBP N102 was successfully grafted onto the surface of CNTs, and the modification of CNTs was successful. To further confirm the success of modification, XPS experiments were carried out on CNTs, CNTs-H202, and CNTs-N102.

*3.1.2. XPS.* To confirm the successful grafting of HBP H202 and HBP N102 onto the surface of CNTs, XPS analysis was performed on CNTs, CNTs-H202, HBP H202, CNTs-N102, and HBP N102, and the results are shown in Figure 2. After calculation, the relative concentrations of $C_{1s}$, $N_{1s}$, and $O_{1s}$ of the samples are shown in Table 1.

**Table 1. Element Contents of CNTs, CNTs-H202, HBP H202, CNTs-N102, and HBP N102**

| samples | $C_{1s}$ (%) | $N_{1s}$ (%) | $O_{1s}$ (%) |
|---|---|---|---|
| CNTs | 97.66 | 0 | 2.34 |
| CNTs-H202 | 86.91 | 0 | 13.09 |
| HBP H202 | 68.22 | 0 | 31.78 |
| CNTs-N102 | 95.21 | 2.14 | 2.65 |
| HBP N102 | 52.24 | 29.39 | 18.37 |

As shown in Figure 2a, after modification, CNTs-H202 has a stronger peak of $O_{1s}$, which is due to the fact that the HBP H202 had successfully grafted on the surface of CNTs. And according to the element contents, compared with CNTs and CNTs-H202, the raise of the O element also confirms the success of modification.

As shown in Figure 2b, the results show that CNTs before modification did not contain N. After surface modification with HBP N102 containing sufficient amino groups, the $N_{1s}$ peak appeared in CNTs-N102, indicating that HBP N102 was successfully grafted onto the surface of CNTs. On the basis of the element concentration, it can also be concluded that the successful grafting of HBP N102 resulted in the introduction of N into CNTs.

*3.1.3. TGA.* To further confirm the success of the modification and the grafting amount of HBP, TGA was performed on CNTs, modified CNTs, and HBPs, and the results are shown in Figure 3. From Figure 3a, it can be observed that the weight loss of HBP H202 mainly occurred in


https://doi.org/10.1021/acsomega.2c05104
ACS Omega 2022, 7, 42939−42948

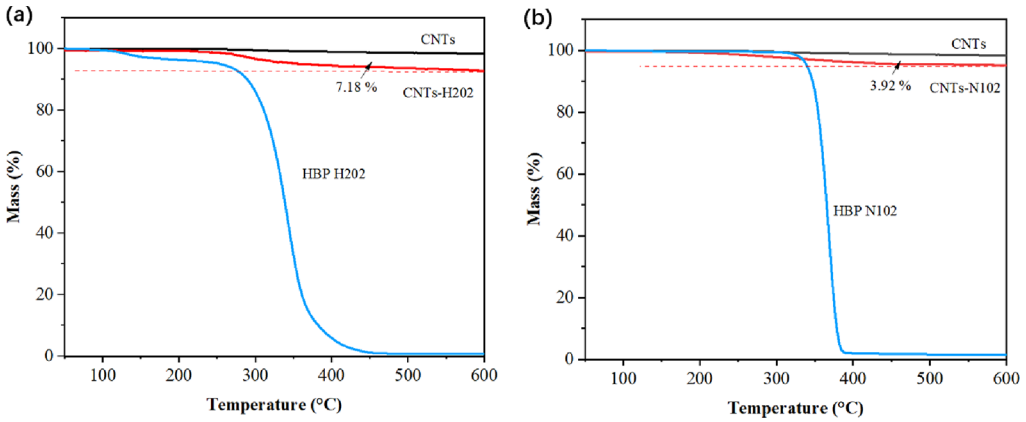


**Figure 3.** (a) TGA plot of CNTs, CNTs-H202, and HBP H202. (b) TGA plot of CNTs, CNTs-N102, and HBP N102.

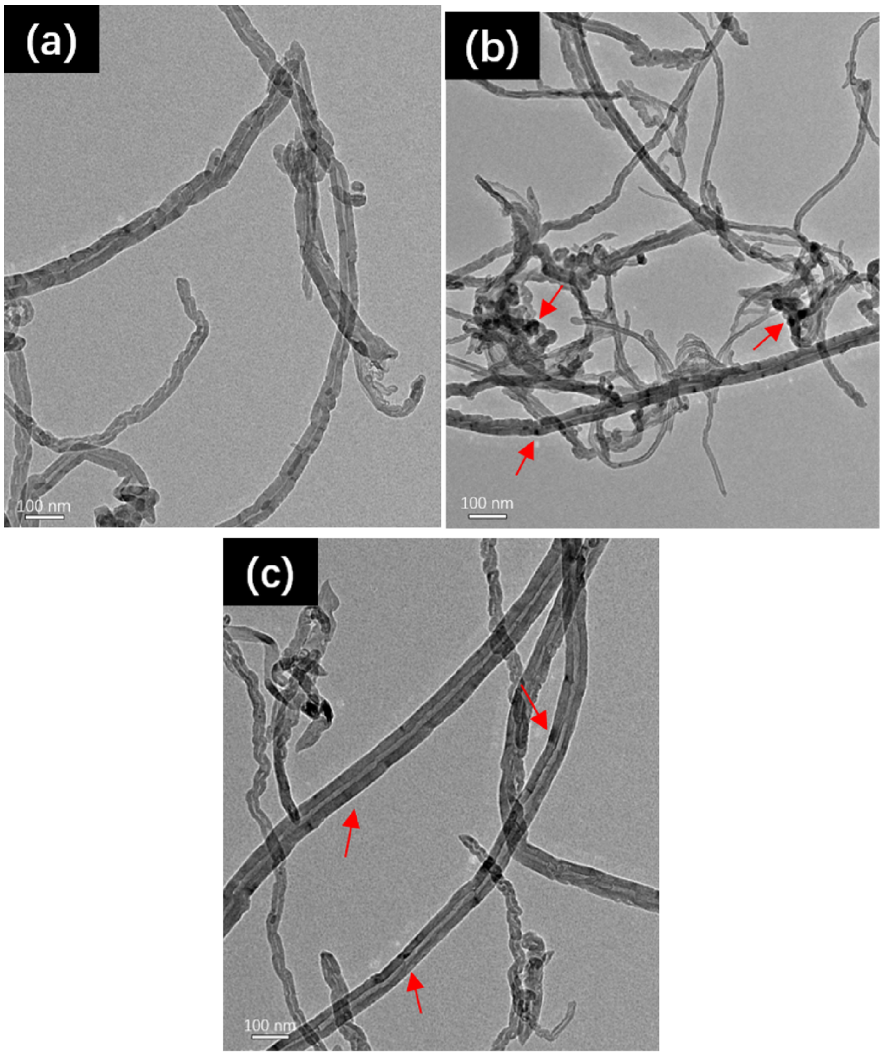


**Figure 4.** TEM images of (a) CNTs, (b) CNTs-H202, and (c) CNTs-N102.

two steps, and the maximum weight loss temperature was 131.4 and 344.2 °C, respectively. For the raw CNTs, because of their high thermal stability, no significant weight loss can be observed in the temperature range of 50−600 °C. Therefore, the residual content at 600 °C can be considered to be 100%.[27] For CNTs-H202, the maximum weight loss temperature is 302 °C, indicating that HBP H202 had been grafted onto CNTs. In addition, a weight loss of 7.18% is seen at 450 °C, which means that the grafting amount of HBP H202 can be roughly estimated to be 7.18%.

As can be seen from Figure 3b, the thermal weight loss of modified CNTs occurs in the same temperature range, starting from about 150 °C and ending at about 450 °C. Compared with HBP H202, HBP N012 has a narrower thermal weight



https://doi.org/10.1021/acsomega.2c05104
ACS Omega 2022, 7, 42939−42948

loss temperature range, roughly 320−390 °C. Similarly, the maximum weight loss temperature of CNT-N102 was 372.7 °C, which also means that HBP N102 was successfully grafted onto the surface of CNTs. Through TGA analysis, we concluded that the grafting rate of CNT-N102 was 3.92%.

The grafting rate of HBPs is an important characterization of the modification effect of CNTs and an important factor affecting the regulation of modified CNTs on the crystallization performance of PLLA. The grafting rate of HBP is influenced by the molecule weight of HBPs and the dispersity of HBP in matrix materials.[27] As mentioned above, the HBPs we selected were of similar molecular weight. Therefore, the difference of grafting rate is caused by the different dispersity of HBPs in PLLA. In HBP H202, the terminal group is −OH, and there are a large number of −COO− groups in the molecular chain. However, in N102, the terminal group is $-NH_2$, and the molecular chain is connected by −CONH−. As we know, PLLA is a linear polyester structure, so we believe that HBP H202 has better compatibility and dispersion in PLLA.

*3.1.4. TEM.* To explore the changes of the surface morphology of CNTs before and after modification, a TEM test was performed. The TEM results of unmodified and modified CNTs are shown in Figure 4. Figure 4a shows the surface morphology of unmodified CNTs. Figures 4b,c shows the surface morphology of CNTs-H202 and CNTs-N102, respectively. It can be seen that because of the grafting of HBP, many black dots marked by arrows appear on its surface. In conclusion, the surface morphology of CNTs was changed by the addition of HBP.

*3.1.5. WAXD.* To study the structure change of modified CNTs, WAXD measurements were conducted. The diffraction patterns of pure and modified CNTs are shown in Figure 5.

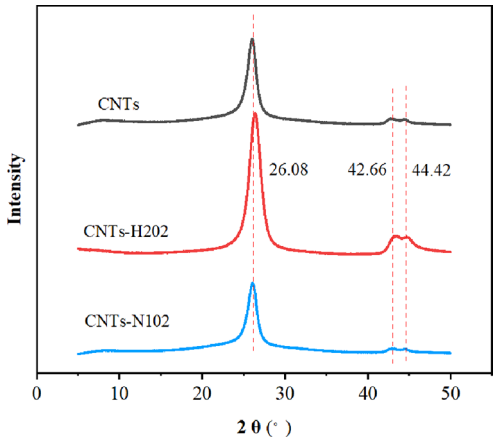


**Figure 5.** WAXD spectrum of CNTs, CNTs-H202, and CNTs-N102.

The diffraction peaks of the modified CNTs do not change significantly after modification. The diffraction peaks of (002), (100), and (101) are 26.0, 42.7, and 44.4° at $2\theta$ angles, respectively, and the calculated crystal plane spacing of (002) is 3.41 Å. After grafting, the spacing between crystal planes at the same position did not change much because the surface modification would not destroy the structure of CNTs, thus ensuring the structural integrity of CNTs. In this way, the modified CNTs could be used as the nucleating agent as pure CNTs on the crystallization of PLLA.

**3.2. Crystallization Behavior of PLLA/CNT Composites.** *3.2.1. DSC.* To study the crystallization properties of PLLA and PLLA/CNTs, DSC measurements were conducted. The calorimetric curves of the test results are shown in Figure 6. The calorimetric parameters, including the crystallization peak temperature $T_c$, crystallization enthalpy in the cooling process ("enthalpy" in Table 2), peak temperature of cold crystallization $T_{cc}$, enthalpy of cold crystallization $\Delta H_{cc}$ in the melting process, enthalpy of fusion $\Delta H_m$, and relative degree of crystallinity $X$, are shown in Table 2.[28−31]

As shown in Figure 6a, there is no obvious peak in pure PLLA during the cooling process, while obvious peaks appear in the cooling curve of samples after the addition of CNTs, indicating that the addition of CNTs promotes the crystallization of PLLA. At the same time, the crystallization peak temperature $T_c$ and cooling crystallization enthalpy shown in Table 2 also indicate that the addition of CNTs greatly promoted the crystallization performance of PLLA. Compared with unmodified CNTs, the modified CNTs show stronger peaks in cooling curves, and the increase of $T_c$ and enthalpy indicates that the modified CNTs have better regulation on the crystallization of PLLA.

It can be seen from Figure 6b, in the melting process, that the glass transition peaks appear in all samples at about 65 °C, indicating that the addition of unmodified or modified CNTs has no significant effect on the chemical properties of PLLA. Furthermore, the addition of unmodified and modified CNTs degrades the cold crystallization peaks, indicating that the addition of CNTs promotes the crystallization of PLLA. It is worth noting that the composite PLLA/C-N has hardly any cold crystallization peaks, which means that CNTs-N102 has the best promotion on the crystallization of PLLA.

It can be seen from Table 2 that during the melting process, the peak temperature of cold crystallization $T_{cc}$ and the $\Delta H_{cc}$ decreased owing to the increase of crystallization capacity, indicating that the addition of CNTs promotes the crystallization of PLLA, as shown in Figure. 6b. The $\Delta H_m$ of PLLA and its composites was calculated by integrating the melting exothermic peak. We also calculated the relative degree of crystallinity of PLLA and its composites. The results show that the modified CNTs have better improvement of the relative degree of crystallinity of PLLA, which is about a 64% increase. Furthermore, according to the relative degree of crystallinity, CNTs-H202 and CNTs-N102 have a similar improvement effect on the crystallization properties of PLLA, and CNTs-N102 has only a slight advantage.

To further explore the effect of CNT modification on the crystallization properties of PLLA, isothermal crystallization experiments were carried out. The DSC results and the half crystallization times ($t_{1/2}$) are shown in Figures 7 and 8, respectively. The results show that the addition of CNTs greatly improved the crystallization capacity of PLLA and reduced the crystallization time by nearly half. In addition, the isothermal crystallization has a similar regularity of the crystallization processs and subsequent melting process for different composites, in which CNTs-H202 and CNTs-N102 have a similar improvement effect on the crystallization properties of PLLA and CNTs-N102 has only a weak advantage.

As for the regulation of crystallization properties of PLLA by CNTs, previous studies showed that the crystallization promotion ability was determined by the remaining carboxyl groups on the surface of CNTs. The higher the content of


https://doi.org/10.1021/acsomega.2c05104
ACS Omega 2022, 7, 42939−42948

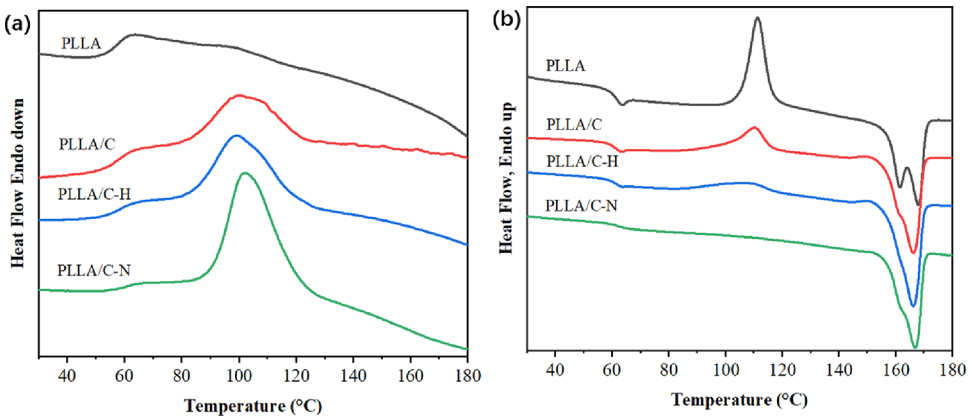


**Figure 6.** Calorimetric curve of PLLA and PLLA/CNT composites: (a) cooling curves and (b) subsequent melting curves.

**Table 2. Calorimetric Parameters of PLLA and PLLA/CNTs Composites**

| | crystallization process | | | subsequent melting process | | |
|---|---|---|---|---|---|---|
| samples | $T_c$ (°C) | enthalpy (J/g) | $T_{cc}$ (°C) | $\Delta H_{cc}$ (J/g) | $\Delta H_m$ (J/g) | $X$ (%) |
| PLLA | 99.2 | 1.8 | 111.5 | 28.6 | 33.8 | 5.6 |
| PLLA/C | 99.8 | 17.0 | 110.4 | 15.2 | 35.0 | 21.2 |
| PLLA/C-H | 99.9 | 26.0 | 106.3 | 6.6 | 36.8 | 32.3 |
| PLLA/C-N | 102.4 | 31.9 | 99.1 | 1.2 | 33.7 | 34.7 |

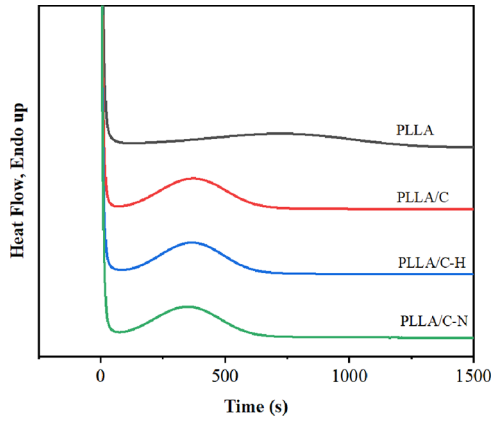


**Figure 7.** Isothermal crystallization curves of PLLA and PLLA/CNT composites.

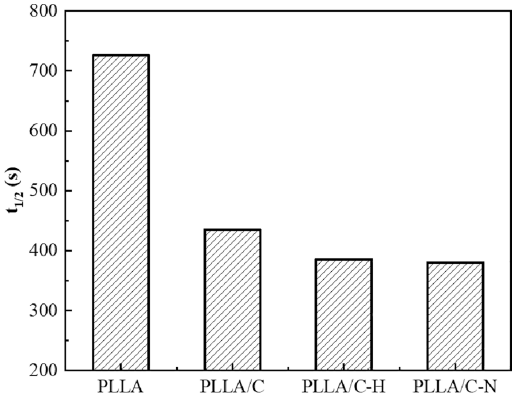


**Figure 8.** Half crystallization times ($t_{1/2}$) of PLLA and PLLA/CNT composites.

residual carboxyl groups is, the better is the crystallization promotion ability of the modified CNTs. According to TGA results, HBP N102 has a lower grafting rate than HBP H202, which also resulted in more carboxyl groups on the surface of CNTs-N102, so it had a better effect on the improvement of the crystallization performance of PLLA. However, previous studies have shown that we can regulate the grafting rate of HBP on the surface of CNTs by adjusting the molecular weight of HBP.[23]

*3.2.2. WAXD.* Figure 9 is the one-dimensional WAXD diffraction pattern after isothermal crystallization at 120 ° C for

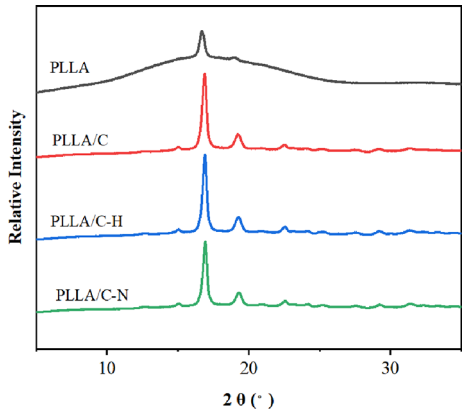


**Figure 9.** WAXD spectrum of PLLA and PLLA/CNT composites.

10 min. First, it can be seen that pure PLLA has a huge amorphous peak at 120 ° C isothermal crystallization for 10 min, indicating that the crystallization ability of pure PLLA is relatively weak. In contrast, the crystallization peak is sharp and the amorphous peak disappears after the nucleating agent is added (modified and unmodified CNTs), indicating that the crystallization of PLLA is greatly improved by adding the nucleating agent.

*3.2.3. PLOM.* The PLOM images are shown in Figure 10. In the isothermal crystallization process, the samples were melted at 200 °C and kept for 8 min to melt completely, and then isothermal crystallization was performed at 120 °C, which was observed over time by a polarizing microscope. As shown in Figure 10a, the grain size of pure PLLA is 42.5 $\mu$m, and compared with the PLLA composites, the nucleation point is less and the grain size is larger, which also leads to the brittleness of PLLA. The crystallization time of PLLA is long,


https://doi.org/10.1021/acsomega.2c05104
ACS Omega 2022, 7, 42939−42948

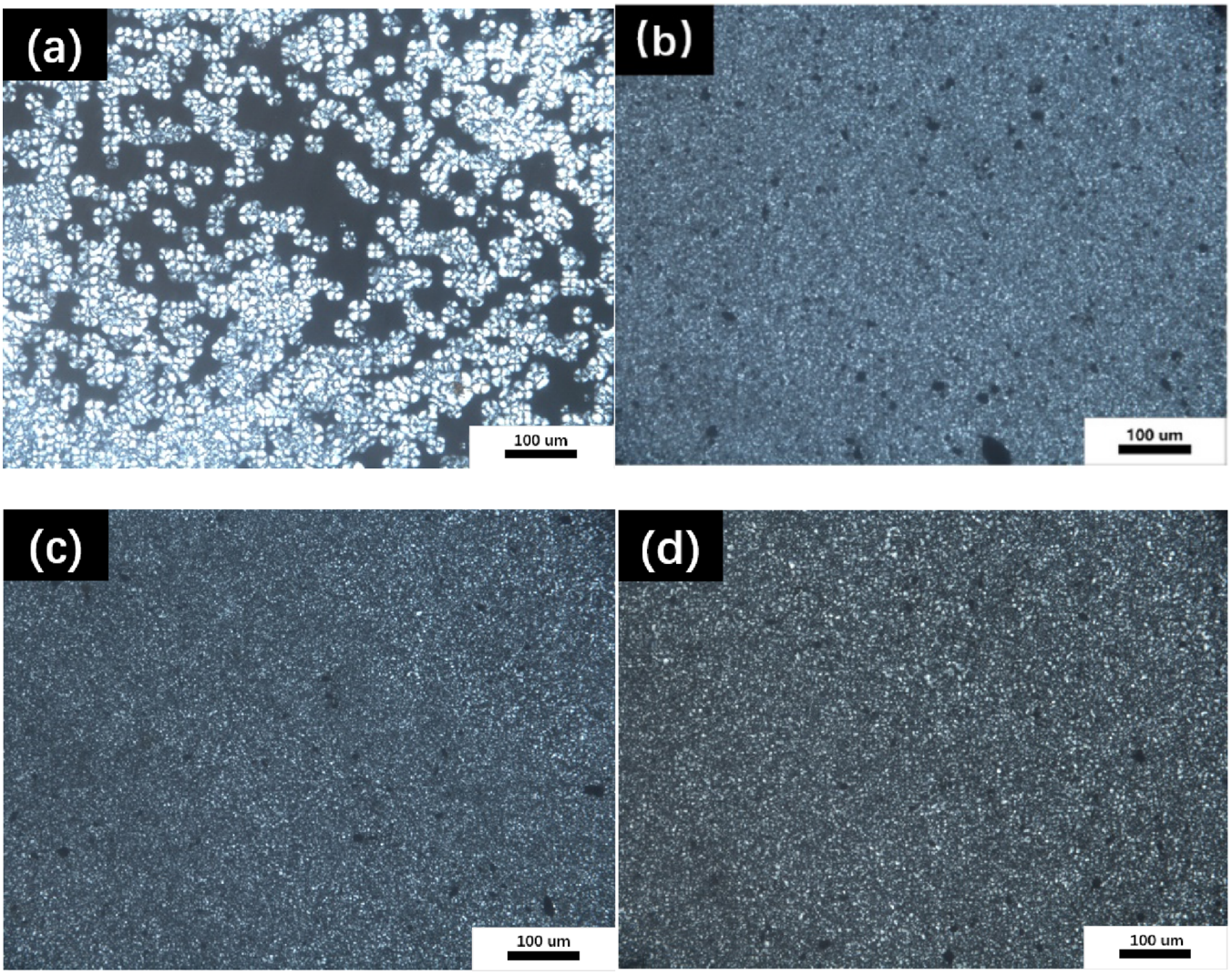


**Figure 10.** PLOM images of the samples after isothermal crystallization: (a) PLLA, (b) PLLA/C, (c) PLLA/C-H, and (d) PLLA/C-N.

and it took about 20 min to completely crystallize. As shown in Figure 10b, the nucleation point increased significantly and the grains were refined after the addition of unmodified CNTs. The grain size and crystallization time are greatly reduced. The grain size is 14 $\mu$m, and the crystallization completion time is reduced to 8 min. However, after the crystallization of unmodified CNTs is completed, there also were some unnucleated points, which were caused by the high surface energy of unmodified CNTs. And when CNTs are directly blended with the PLLA matrix, agglomeration phenomenon will occur and they cannot be dispersed uniformly, resulting in the degradation of their nucleation performance and the vacancy of nucleation point. As shown in Figure 10c, after the addition of CNTs-H202, the grain was further refined with a typical grain size of 11 $\mu$m. However, compared with Figure 10d, there are still few unnucleated points in PLLA/C-H composite, which are due to the fact that the HBP H202 modified CNTs had slight aggregation.

### 3.3. Mechanical Properties of PLLA/CNT Composites.

The stress−strain curves are shown in Figure 11. The stress−strain curves of pure PLLA and PLLA/CNT composites are a similar form, and the addition of unmodified and modified CNTs causes the enhancement of tensile strength of PLLA. We compared the tensile strength, tensile modulus, and elongation at break of PLLA and its composites in Figure 12. The results show that, first, the modification of CNTs results in the improvement of mechanical properties of PLLA, i.e., 10.2% increase in the tensile strength and 12.9% increase in the tensile modulus. Second, PLLA/C-H has better mechanical

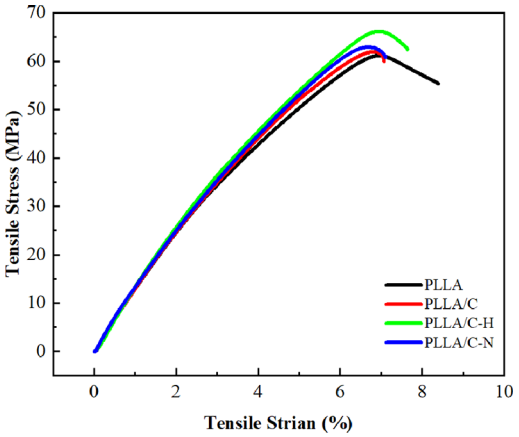


**Figure 11.** Stress−strain curves of PLLA and PLLA/CNT composites.



https://doi.org/10.1021/acsomega.2c05104
ACS Omega 2022, 7, 42939−42948

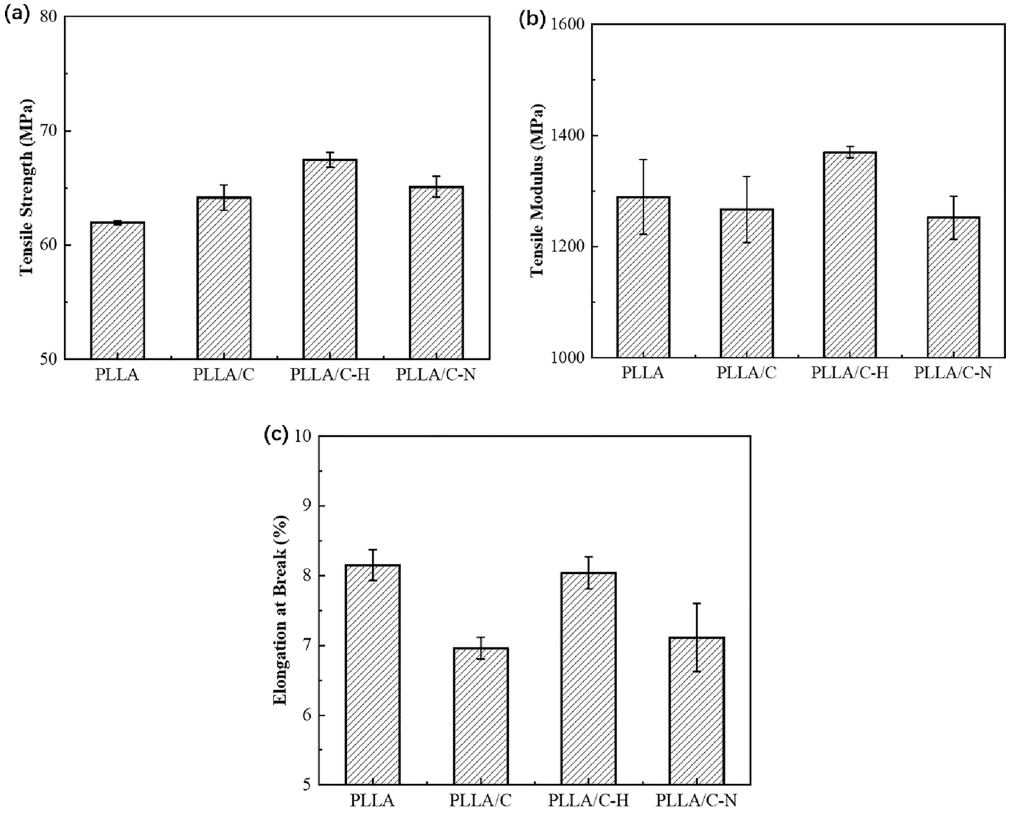


**Figure 12.** The (a) tensile strength, (b) tensile modulus, and (c) elongation at break of PLLA and PLLA/CNT composites.

properties than PLLA/C-N, which are caused by the surface grafted hydroxy-terminated hyperbranched polyesters having better compatibility with PLLA.

## 4. CONCLUSIONS

In this paper, CNTs modified with HBP H202 and HBP N102 were prepared by condensation reaction and amidation reaction, respectively. The modification results were characterized by FTIR, XPS, TGA, SEM, and WAXD. PLLA and PLLA/CNT composites were prepared ,and their crystallization and melting kinetics and mechanical properties were studied. The results showed that, first, the modified CNTs had a better promotion on PLLA crystallization and mechanical properties than the unmodified CNTs. Second, CNTs-N102 had a slight advantage on the promotion on PLLA crystallization, which was caused by the lower grafting rate of HBP N102. Moreover, CNTs-H202 had a better promotion on the mechanical properties of PLLA, which was caused by the better compatibility with PLLA. In conclusion, hydroxy-terminated HBP is a better CNT modified material than amino-terminated HBP, which is due to its better compatibility with PLLA, and CNTs modified by hydroxy-terminated HBP can effectively promote the crystallization and mechanical properties of PLLA.

## AUTHOR INFORMATION


### Corresponding Authors

**Zhihui Xie** − *Dongfang Electric Machinery Co., Ltd., Deyang 618000, China*; Email: xiezhihui123@163.com

**Jian Kang** − *State Key Laboratory of Polymer Materials Engineering, Polymer Research Institute of Sichuan University, Chengdu 610065, China*; orcid.org/0000-0002-3888-2462; Email: jiankang@scu.edu.cn

### Authors

**Bofan Shen** − *State Key Laboratory of Polymer Materials Engineering, Polymer Research Institute of Sichuan University, Chengdu 610065, China*

**Yuxin Xu** − *College of Information & Electrical Engineering, Hebei University of Engineering, Handan, Hebei 056038, China*

**Yue Zhang** − *Dongfang Electric Machinery Co., Ltd., Deyang 618000, China*

**Fuyi Zhang** − *State Key Laboratory of Polymer Materials Engineering, Polymer Research Institute of Sichuan University, Chengdu 610065, China*

**Ya Cao** − *State Key Laboratory of Polymer Materials Engineering, Polymer Research Institute of Sichuan University, Chengdu 610065, China*

**Ming Xiang** − *State Key Laboratory of Polymer Materials Engineering, Polymer Research Institute of Sichuan University, Chengdu 610065, China*

Complete contact information is available at: https://pubs.acs.org/10.1021/acsomega.2c05104



### Funding

This research was funded by National Natural Science Foundation of China (NSFC, Grants 51503134 and 51702282) and State Key Laboratory of Polymer Materials Engineering (Grant SKLPME 2017-3-02), and the APC was funded by the National Natural Science Foundation of China (NSFC, Grant 51702282).

### Notes

The authors declare no competing financial interest.

## ■ ACKNOWLEDGMENTS

We are grateful to the Analytical and Testing Center of Sichuan University for providing XPS and TEM measurement.

## ■ REFERENCES

(1) Iwata, T. Biodegradable and bio-based polymers: future prospects of eco-friendly plastics. *Angew. Chem., Int. Ed. Engl.* **2015**, *54*, 3210−3215.
(2) Lasprilla, A. J. R.; Martinez, G. A. R.; Lunelli, B. H.; Jardini, A. L.; Filho, R. M. Poly-lactic acid synthesis for application in biomedical devices - a review. *Biotechnol. Adv.* **2012**, *30*, 321−328.
(3) Muller, J.; González-Martínez, C.; Chiralt, A. Combination of Poly(lactic) Acid and Starch for Biodegradable Food Packaging. *Materials* **2017**, *10*, 952.
(4) Bhagia, S.; Bornani, K.; Agrawal, R.; Satlewal, A.; Ďurkovič, J.; Lagaňa, R.; Bhagia, M.; Yoo, C. G.; Zhao, X.; Kunc, V.; Pu, Y.; Ozcan, S.; Ragauskas, A. J. Critical review of FDM 3D printing of PLA biocomposites filled with biomass resources, characterization, biodegradability, upcycling and opportunities for biorefineries. *Appl. Mater. Today* **2021**, *24*, No. 101078.
(5) Cocca, M.; Androsch, R.; Righetti, M. C.; Malinconico, M.; Di Lorenzo, M. L. Conformationally disordered crystals and their influence on material properties: The cases of isotactic polypropylene, isotactic poly(1-butene), and poly(l-lactic acid). *J. Mol. Struct.* **2014**, *1078*, 114−132.
(6) Ma, B.; Wang, X.; He, Y.; Dong, Z.; Zhang, X.; Chen, X.; Liu, T. Effect of poly(lactic acid) crystallization on its mechanical and heat resistance performances. *Polymer* **2021**, *212*, No. 123280.
(7) Liu, J.-H.; Huang, M.-L.; Tao, J.-R.; Weng, Y.-X.; Wang, M. Fabrication of recyclable nucleating agent and its effect on crystallization, gas barrier, thermal, and mechanical performance of Poly( −lactide). *Polymer* **2021**, *231*, No. 124121.
(8) Shi, X.; Zhang, G.; Phuong, T.; Lazzeri, A. Synergistic effects of nucleating agents and plasticizers on the crystallization behavior of poly(lactic acid). *Molecules* **2015**, *20*, 1579−1593.
(9) Rathinavel, S.; Priyadharshini, K.; Panda, D. A review on carbon nanotube: An overview of synthesis, properties, functionalization, characterization, and the application. *Mater. Sci. Eng., B* **2021**, *268*, No. 115095.
(10) Raphey, V. R.; Henna, T. K.; Nivitha, K. P.; Mufeedha, P.; Sabu, C.; Pramod, K. Advanced biomedical applications of carbon nanotube. *Mater. Sci. Eng., C* **2019**, *100*, 616−630.
(11) Sun, Y.; Hou, K.; Zhang, D.; Chang, S.; Ye, L.; Cao, A.; Shang, Y. High performance carbon nanotube/polymer composite fibers and water-driven actuators. *Compos. Sci. Technol.* **2021**, *206*, No. 108676.
(12) Kim, S. Y.; Shin, K. S.; Lee, S. H.; Kim, K. W.; Youn, J. R. Unique crystallization behavior of multi-walled carbon nanotube filled poly(lactic acid). *Fibers Polym.* **2010**, *11*, 1018−1023.
(13) Yu, Z.; Jiang, Z.; Qiu, Z. In-situ synthesis and thermal properties of biobased Poly(neopentyl glycol 2,5-furandicarboxylate)/multi-walled carbon nanotubes composites. *Polymer* **2021**, *229*, No. 124019.
(14) Wang, L.; Qiu, J.; Sakai, E.; Wei, X. The relationship between microstructure and mechanical properties of carbon nanotubes/polylactic acid nanocomposites prepared by twin-screw extrusion. *Composites, Part A* **2016**, *89*, 18−25.
(15) Goutianos, S.; Peijs, T. On the low reinforcing efficiency of carbon nanotubes in high-performance polymer fibres. *NANO* **2021**, *7*, 53−69.
(16) David, M. E.; Ion, R. M.; Grigorescu, R. M.; Iancu, L.; Constantin, M.; Stirbescu, R. M.; Gheboianu, A. I. Wood Surface Modification with Hybrid Materials Based on Multi-Walled Carbon Nanotubes. *Nanomaterials* **2022**, *12*, 1990.
(17) Wilms, D.; Stiriba, S. E.; Frey, H. Hyperbranched polyglycerols: from the controlled synthesis of biocompatible polyether polyols to multipurpose applications. *Acc. Chem. Res.* **2010**, *43*, 129−141.
(18) Feng, L.; Li, R.; Yang, H.; Chen, S.; Yang, W. The Hyperbranched Polyester Reinforced Unsaturated Polyester Resin. *Polymer* **2022**, *14*, 1127.
(19) Nyambo, C.; Misra, M.; Mohanty, A. K. Toughening of brittle poly(lactide) with hyperbranched poly(ester-amide) and isocyanate-terminated prepolymer of polybutadiene. *J. Mater. Sci.* **2012**, *47*, 5158−5168.
(20) Sun, J.; Jin, Y.; Wang, B.; Tian, H.; Kang, K.; Men, S.; Weng, Y. High-toughening modification of polylactic acid by long-chain hyperbranched polymers. *J. Appl. Polym. Sci.* **2021**, *138*, 51295.
(21) Morancho, J. M.; Fernández-Francos, X.; Acebo, C.; Ramis, X.; Salla, J. M.; Serra, À. Thermal curing of an epoxy-anhydride system modified with hyperbranched poly(ethylene imine)s with different terminal groups. *J. Therm. Anal. Calorim.* **2017**, *127*, 645−654.
(22) Park, H. S.; Hong, C. K. Relationship between the Stereocomplex Crystallization Behavior and Mechanical Properties of PLLA/PDLA Blends. *Polymer* **2021**, *13*, 1851.
(23) Shen, B.; Lu, S.; Sun, C.; Song, Z.; Zhang, F.; Kang, J.; Cao, Y.; Xiang, M. Effects of Amino Hyperbranched Polymer-Modified Carbon Nanotubes on the Crystallization Behavior of Poly (L-Lactic Acid) (PLLA). *Polymer* **2022**, *14*, 2188.
(24) Okpalugo, T. I. T.; Papakonstantinou, P.; Murphy, H.; McLaughlin, J.; Brown, N. M. D. High resolution XPS characterization of chemical functionalised MWCNTs and SWCNTs. *Carbon* **2005**, *43*, 153−161.
(25) Tsuji, H. Properties and morphologies of poly(?-lactide): 1. Annealing condition effects on properties and morphologies of poly(?-lactide). *Polymer* **1995**, *36*, 2709−2716.
(26) Zhang, F.; Jiang, W.; Song, X.; Kang, J.; Cao, Y.; Xiang, M. Effects of Hyperbranched Polyester-Modified Carbon Nanotubes on the Crystallization Kinetics of Polylactic Acid. *ACS Omega* **2021**, *6*, 10362−10370.
(27) Han, C.; Zhang, X.; Chen, D.; Ma, Y.; Zhao, C.; Yang, W. Enhanced dielectric properties of sandwich-structured biaxially oriented polypropylene by grafting hyper-branched aromatic polyamide as surface layers. *J. Appl. Polym. Sci.* **2020**, *137*, 48990.
(28) Yu, Y.; Jiang, X.; Fang, Y.; Chen, J.; Kang, J.; Cao, Y.; Xiang, M. Investigation on the Effect of Hyperbranched Polyester Grafted Graphene Oxide on the Crystallization Behaviors of $\beta$-Nucleated Isotactic Polypropylene. *Polymer* **2019**, *11*, 1988.
(29) Li, Y.; Liu, H.; Huang, X.; Song, X.; Kang, J.; Chen, Z.; Zeng, F.; Chen, J. Investigation on the Roles of $\beta$-Nucleating Agents in Crystallization and Polymorphic Behavior of Isotactic Polypropylene. *Polym. Sci., Ser. A* **2020**, *62*, 470−480.
(30) Jiang, W.; Song, X.; Zhou, R.; Wu, Z.; Hu, B.; Zhang, Y.; Liang, Z.; Chen, Z.; Kang, J.; Xiang, M. Influences of molecular structure on the isothermal crystallization behavior and mechanical properties of $\beta$-nucleated isotactic polypropylene. *Polym.-Plast. Technol. Mater.* **2020**, *59*, 1724−1735.
(31) Wu, D.; Wu, L.; Wu, L.; Xu, B.; Zhang, Y.; Zhang, M. Nonisothermal cold crystallization behavior and kinetics of polylactide/clay nanocomposites. *J. Polym. Sci., Part B: Polym. Phys.* **2007**, *45*, 1100−1113.



https://doi.org/10.1021/acsomega.2c05104
*ACS Omega* 2022, 7, 42939−42948